Enhancing higher harmonics of a tapping cantilever by excitation at a submultiple of its resonance frequency

M. Balantekin* and A. Atalar
Bilkent University, Electrical Engineering Department, Bilkent, TR-06800, Ankara, Turkey
(Received 24 May 2004; revised manuscript received 25 October 2004; published 22 March 2005)

In a tapping-mode atomic force microscope, the frequency spectrum of the oscillating cantilever contains higher harmonics at integer multiples of the excitation frequency. When the cantilever oscillates at its fundamental resonance frequency w_1, the high Q-factor damps the amplitudes of the higher harmonics to negligible levels, unless the higher flexural eigenmodes are coincident with those harmonics. One can enhance the nth harmonic by the Q factor when the cantilever is excited at a submultiple of its resonance frequency (w_1/n). Hence, the magnitude of the nth harmonic can be measured easily and it can be utilized to examine the material properties. We show theoretically that the amplitude of enhanced higher harmonic increases monotonically for a range of sample stiffness, if the interaction is dominated by elastic force.

DOI: 10.1103/PhysRevB.71.125416 PACS number(s): 68.37.Ps, 62.20.Dc

I. INTRODUCTION

The determination of sample elasticity at a nanometer scale has been a goal of many researchers.[1–16] The nanoindentation,[1] force modulation,[2] atomic force acoustic microscopy,[3] or ultrasonic force microscopy[4] are the methods developed so far to characterize the local elastic properties of samples. In these methods, the applied static loads degrade the lateral resolution.

It was recently found that the anharmonic oscillations of the cantilever contain information about the material nanomechanical properties.[17–20] Hillenbrand *et al.* used the 13th harmonic signal to increase the image contrast.[18] Some authors used second and third harmonic amplitudes to map the surface charge density of DNA molecules.[21] Dürig realized that the higher harmonic amplitudes can be utilized for the reconstruction of the interaction force.[22] A numerical analysis by Rodriguez and Garcia showed that phase of the second mode can be utilized to map the Hamaker constant.[23] Since the tip-sample interaction is periodic, the frequency spectrum of the detected signal has components (harmonics) at integer multiples of the driving frequency. These harmonics depend on the interaction force and hence the material properties.

In conventional tapping-mode experiments, the higher harmonics are generally ignored and in fact, their amplitudes are two or three orders of magnitude smaller than the fundamental component of oscillation as both numerical[24] and experimental[25] results indicate. The nth harmonic amplitude is related to the nth harmonic of the interaction force f_n via the transfer gain $|H(nw)|$ as follows:

$$A_n = |H(nw) f_n|, \quad \text{for } n \geq 2, \tag{1}$$

where w is the excitation frequency. The transfer function of a rectangular cantilever including higher flexural eigenmodes was obtained by Stark and Heckl.[17]

To increase the nth harmonic amplitude A_n and hence the measurement sensitivity, we must increase either f_n or $|H(nw)|$. Notice that increasing f_n may mean an additional damage to the sample, and therefore it may not be desirable for all kinds of samples. The transfer gains for the higher harmonics in conventional tapping-mode operation ($w = w_1$, where w_1 is the resonant frequency of the first mode) are very small unless the higher harmonic frequencies are coincident with the resonant frequencies of the higher eigenmodes. If we consider only the fundamental eigenmode of a cantilever with a stiffness of k, the transfer gain for the nth harmonic will be $[k(n^2-1)]^{-1}$. This yields a very small value for increasing n. The use of higher harmonics close to the higher transverse resonances can enhance the measurement sensitivity.[26] However, to increase the amplitudes of higher harmonics in this case, one may need to increase the free oscillation amplitude or decrease the set point (damped) amplitude which in turn increases the tip-sample forces.

Most cantilevers do not have eigenmodes at integer multiples of each other. But, it is possible to fabricate special cantilevers, called "harmonic cantilevers," in such a way that one of the eigenmodes is at an integer multiple of the fundamental mode.[27] The recent study by Sahin *et al.* showed that these cantilevers can be used to enhance one of the higher harmonics.[28]

Indeed, measuring the higher harmonic signal sensitivity would give an opportunity to researchers in examining the material properties at nanoscale more effectively. To enhance the quality of the measured harmonic signal, we propose a method which can easily be employed in conventional tapping-mode systems. In the next section, we will describe the method and test it by numerical simulations. The analytical analysis for low harmonic distortion is also provided in an Appendix to provide physical insight.

II. SIMULATIONS OF A NEW HARMONIC ENHANCEMENT METHOD

Considering the fundamental eigenmode, the transfer gain reaches its maximum value (Q/k, where Q is the quality factor) at the first resonance frequency w_1. If we drive the cantilever at a submultiple of w_1, i.e., at $w = w_{1n} = w_1/n$ (n is

 ©2005 American Institute of Physics

an integer number), then, due to the high transfer gain at $nw_{1n}=w_1$, the nth harmonic amplitude is expected to be much larger than the conventional case. This allows us to detect the harmonic signal with a good signal-to-noise ratio and to inspect the tip-sample interaction effectively. To vibrate the cantilever at w_{1n} with a reasonable amplitude, a higher driving force must be applied since there is no Q enhancement for the fundamental component of the oscillation.

To investigate if the proposed method can be helpful for differentiating the stiffness of materials and to analyze the effect of the method on the dynamics of tip-sample system, we performed numerical simulations. The simulations are done by converting the mechanical model into an equivalent electrical circuit[29] containing nonlinear elements. The equivalent circuit is simulated with SPICE, a powerful and easily available circuit simulator. The details of the simulation setup can be found elsewhere.[30] The simulations are done in a time domain with a step size of one thousandth of one period. To make sure that the steady state is reached, $10Q$ oscillation cycles are simulated. We choose a typical cantilever with a stiffness of $k=1$ N/m, a quality factor of $Q=100$, and a fundamental resonance frequency of $w_1=2\pi\times 120$ krad/s. The free oscillation amplitude A_0 and set point amplitude A_1 are chosen to be $A_0=100$ nm and $A_1=0.99A_0$.

In tapping-mode operation, the cantilever tip experiences both attractive surface forces and a repulsive contact force. The attractive part of the interaction force contains the van der Waals and capillary forces.[31] If the elastic repulsive force applied during the contact is much larger than the attractive forces, then one can ignore the attractive forces. We considered only the elastic force in our simulations to find how the enhanced higher harmonics change with sample elasticity even though the attractive forces can easily be included. According to the Hertzian contact mechanics, the normal load F_H is related to the indentation depth δ for any kind of indenter as[8] $F_H=\beta E^*\delta^\alpha$, where E^* is the effective Young's modulus, β and α are the constants dependent on the tip geometry. Usually, the tip end is approximated with a paraboloidal (spherical) shape having a radius of curvature R. In this case, the parameters defining the tip geometry will be $\beta=4\sqrt{R}/3$ and $\alpha=3/2$. In the simulations R is selected to have a typical value of 10 nm.

We analyzed in detail the response of the enhanced second and third harmonic signals as a function of the effective tip-sample elasticity E^*, when the cantilever is driven at the submultiple frequencies of $w=w_{12}=w_1/2$ and $w=w_{13}=w_1/3$. Figure 1 shows the variation of normalized second (A_2/A_0) and third (A_3/A_0) harmonic amplitudes with E^*. This figure is divided into two regions by a dashed vertical line. In region I, the tip stays in contact with the sample more than a half oscillation period, whereas in region II the contact time is less than a half period. The first observation is that the magnitude of the second harmonic signal can reach almost 40% of the fundamental component. Second, it is seen that the higher harmonic amplitudes are increasing monotonically in a certain range of sample stiffness. The second harmonic amplitude is larger than the third harmonic amplitude and the steeply increasing part of the second harmonic amplitude is at a lower elasticity region compared to the third harmonic. Finally, we find that the tip motion can show chaotic behavior at a relatively high elasticity region (marked by a dotted line).

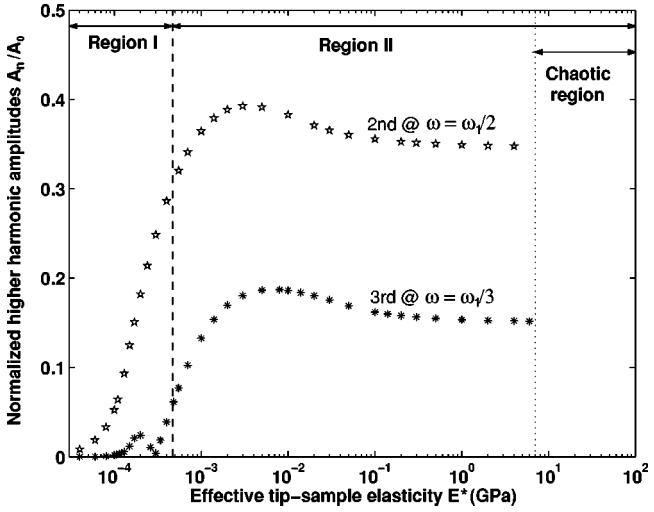

FIG. 1. Simulation results for the second and third harmonics when the cantilever is driven at $w=w_1/2$ and $w=w_1/3$, respectively. A_2/A_0 (stars) and A_3/A_0 (asterisks) are plotted for a paraboloidal tip with a radius of curvature $R=10$ nm. The simulation parameters are $A_0=100$ nm, $A_1/A_0=0.99$, $Q=100$ and $k=1$ N/m. A vertical dashed line separates the region I ($\gamma<0$) and region II ($\gamma>0$), whereas the dotted line indicates the beginning of the chaotic region for the third harmonic. Those locations for the second harmonic are very close to these lines and not shown for clarity.

The phase of the cantilever oscillation can be used to map energy dissipation.[32] On the other hand, it cannot be used to differentiate the compliance of purely elastic samples.[33] In such a case, the enhanced harmonic signal can be useful to increase the image contrast. To map the sample elasticity, the harmonic amplitude variations should be monotonic in a range which covers Young's moduli of the materials under investigation. If we consider region II, it is seen that the samples which have different compliance may not be differentiated and the contrast in the images cannot be interpreted uniquely because of the nonmonotonic variations. Furthermore, there are no steady-state values of harmonic amplitudes for relatively stiff samples due to the chaotic system response. We used a time series analysis software TISEAN[34] to find the largest Lyapunov exponent which indicates whether the system is chaotic or not.[35] The possibility of chaotic system behavior in conventional tapping-mode AFM was predicted by Hunt and Sarid.[36] The numerical analysis by Stark[37] also showed that the chaos can occur depending on the tip-sample gap as the higher harmonics are enhanced by higher eigenmodes.

To gain further insight on the dynamics of the system response, we provided one cycle of tip position graph as obtained from the simulations for three different samples in Fig. 2. It is seen that as the sample gets stiffer, the tip motion deviates heavily from the sinusoidal shape. We can also write the power balance equation to find the relation

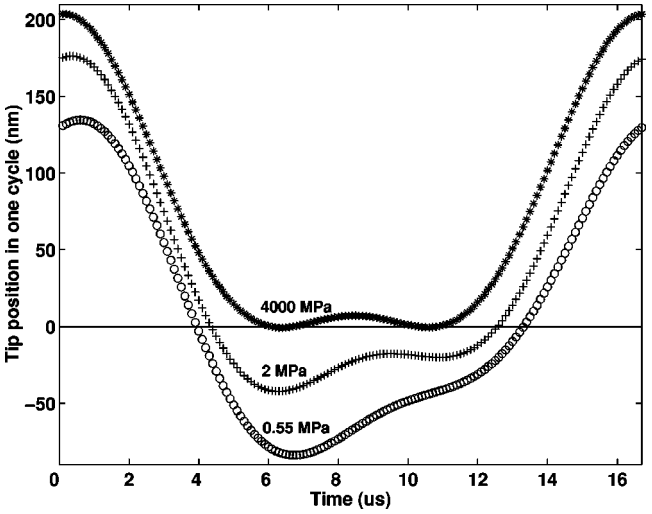

FIG. 2. Tip motions taken from simulations for three different elastic samples when the cantilever is excited at $w=w_1/2$. The position of the undeformed sample surface is indicated by the horizontal line.

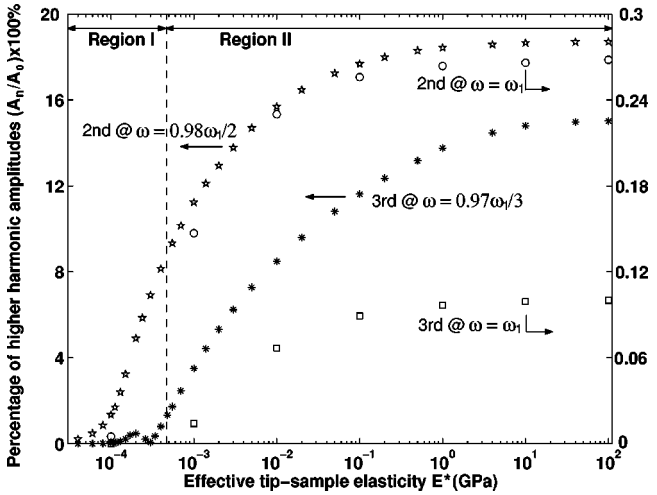

FIG. 3. Left-hand axis: Simulation results for A_2 ($w=0.98w_1/2$) marked by stars and A_3 ($w=0.97w_1/3$) marked by asterisks in the percentage of A_0 with the same parameters of Fig. 1. The vertical dashed line indicates the $\gamma=0$ location. Right-hand axis: Simulation results for the conventional case ($w=w_1$). A_2 is marked by circles and A_3 is marked by rectangles in the percentage of A_0 at $A_1/A_0=0.6$. The other parameters are the same.

between A_n and the system variables. The power input to the system is[32] $kw_{1n}A_dA_1\sin(\phi)/2$, where A_d and ϕ are the drive amplitude and the phase shift between the drive and displacement signals. This power is dissipated partly by the fundamental component of tip oscillation $[kw_{1n}^2A_1^2/(2Qw_1)]$ and partly by the enhanced higher harmonic $[kw_1^2A_n^2/(2Qw_1)]$. We assumed that there is no energy dissipation in the sample and the other (unmatched) higher harmonics are negligible (as obtained from simulations) since A_1/A_0 is set very close to 1. From this balance one can find A_n in terms of ϕ as

$$A_n=(A_1/n)[Q(n-1/n)(A_0/A_1)\sin(\phi)-1]^{1/2}. \qquad (2)$$

In this formulation, we used $A_d\cong(1-w^2/w_1^2)A_0$ which is valid for a high-Q cantilever excited at $w\leqslant w_1/2$. It is found that A_n and ϕ depend on each other. We observed in simulations that ϕ initially increases and after a peak value it decreases as the sample gets stiffer. This explains the nonmonotonic behavior seen in Fig. 1. Equation (2) also helps to explain the observed amplitude differences in second and third harmonics. For a given w_1, as n increases the energy input decreases which in turn limits the amplitude of the nth harmonic.

If the higher harmonic signal A_n becomes a significant fraction of A_0, the relation between A_n and the sample stiffness is no longer monotonic. Moreover, the cantilever can get into chaotic motion if the sample stiffness is very high. To avoid these problems, the enhancement can be reduced by choosing an excitation frequency that is slightly different than the submultiple frequency.

We performed the simulations at slightly shifted excitation frequencies and plotted the results in Fig. 3. For the second harmonic we drive the cantilever at $w=0.98w_{12}$ and for the third harmonic we selected $w=0.97w_{13}$. It is seen that the variations become monotonic in region II and the chaotic behavior is eliminated. The amplitudes saturate for increasing sample stiffness. The saturated amplitudes of second and third harmonics are still more than 15% of A_0 which gives a very good sensitivity. To make a comparison between the harmonic amplitudes of the conventional mode of operation, where the cantilever is excited at $w=w_1$, we performed more simulations and plotted the results in the same figure. We find that the second and third harmonic amplitudes in the conventional case are not more than 0.3% of A_0.

The force applied by the tip on the surface must be carefully chosen for imaging delicate samples. For the same cantilever and tip shape, the parameters that affect the interaction force are the driving frequency[38,39] w, free oscillation amplitude A_0, and the set point ratio A_1/A_0. To enhance the second harmonic, we excite the cantilever at $0.98w_{12}$. A_0 and A_1/A_0 are selected to be 100 nm and 0.99. For the selected parameters, we found that the maximum value of the interaction force is less than 18 nN for the elasticity of samples less than 10 GPa. As a comparison, the maximum applied force is found to be less than 17.6 nN in conventional tapping mode operation ($w=w_1$) with the parameters of $A_0=100$ nm and $A_1/A_0=0.6$ and for the same range of sample elasticity. Note that the force applied to the surface in a conventional case will be less than 5.5 nN if we select $A_1/A_0=0.99$, in which case the higher harmonic amplitudes will be less than 0.05% of A_0. Here, we selected A_1/A_0 to be 0.6 to make a fair comparison between the higher harmonic amplitudes of two cases. Hence, we conclude that higher harmonic amplitudes of the proposed method are much larger than that of the conventional case even though the same forces are applied to the surface.

III. CONCLUSIONS

We showed that the higher harmonic amplitudes can be enhanced by exciting the cantilever at a submultiple of fun-

damental resonance. With this method, the most sensitive portion of the cantilever transfer function is utilized for the detection of harmonic amplitudes. We demonstrated that the amplitude of the enhanced higher harmonics is almost monotonically related to sample elasticity. In tapping-mode operation, the lateral forces are reduced significantly and therefore harmonic imaging offers a higher image resolution compared to the previously developed elasticity imaging methods.

APPENDIX: ANALYTICAL APPROXIMATION FOR LOW HARMONIC DISTORTION

In tapping-mode operation, as the tip taps on an elastic sample, it indents periodically into the sample during the contact. If we assume that the sinusoidal nature of the tip motion is preserved (low harmonic distortion), then the indentation depth is also sinusoidal in the contact duration τ. For a given set point amplitude A_1, mean tip to surface separation z_r and excitation frequency w, we can express the time-dependent interaction force $f_{\mathbf{TS}}(t)$ in one period if $|z_r| \leqslant A_1$ as

$$f_{\mathbf{TS}}(t) = \begin{cases} \beta E^*[A_1 \cos(wt) - z_r]^\alpha & \text{for } |t| \leqslant \cos^{-1}(z_r/A_1)/w \\ 0, & \text{otherwise.} \end{cases} \tag{A1}$$

If $z_r > A_1$ then $f_{\mathbf{TS}}(t) = 0$ and if $z_r < -A_1$ then $f_{\mathbf{TS}}(t) = \beta E^*[A_1 \cos(wt) - z_r]^\alpha$.

For a tip having a conical shape, the parameter defining the tip geometry is the semivertical angle θ [$\beta = 2\tan(\theta)/\pi$, $\alpha = 2$]. Defining a normalized mean tip to surface distance γ as $\gamma = z_r/A_1$, the maximum force applied to the sample is found to be

$$F_{\max} = 2\tan(\theta) E^* A_1^2 (1-\gamma)^2/\pi. \tag{A2}$$

In the steady state, the interaction force can be expanded in a Fourier series[17,40] as $f_{\mathbf{TS}}(t) = f_0 + \Sigma_{n\geqslant 1} f_n \cos(nwt)$. For $|\gamma| \leqslant 1$, the average force f_0 is given by

$$f_0 = F_{\max}\xi \frac{0.5 + \gamma^2 + 0.5\,\mathrm{sinc}(2\xi) - 2\gamma\,\mathrm{sinc}(\xi)}{(1-\gamma)^2}, \tag{A3}$$

where $\mathrm{sinc}(x) \triangleq \sin(\pi x)/(\pi x)$. $\xi = \cos^{-1}(\gamma)/\pi$ is the normalized contact time, i.e., the contact time divided by one period ($w\tau/2\pi$). The fundamental and higher order force components are found using

$$f_n = 2F_{\max}\xi \frac{h_n(\gamma)}{(1-\gamma)^2}, \tag{A4}$$

where $h_n(\gamma)$ is given by

$$h_n(\gamma) = -\gamma\{\mathrm{sinc}[(1+n)\xi] + \mathrm{sinc}[(1-n)\xi]\} + (0.5+\gamma^2) \times \mathrm{sinc}(n\xi) + 0.25\{\mathrm{sinc}[(2+n)\xi] + \mathrm{sinc}[(2-n)\xi]\}. \tag{A5}$$

f_1 causes an amplitude damping[30] and can be related to oscillation amplitude and cantilever parameters under the assumption of low harmonic distortion as follows:

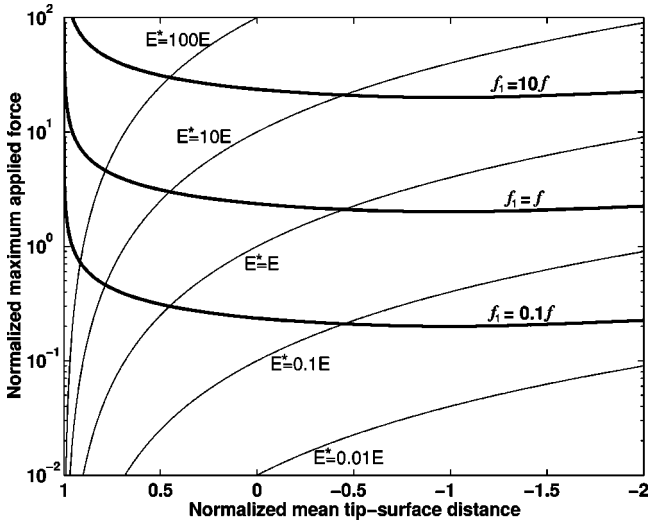

FIG. 4. Normalized maximum repulsive force $F_{\max}/(\beta A_1^\alpha E)$ (thin lines) and $F_{\max}/f$ (thick lines) are plotted as a function of normalized mean tip-surface distance γ for varying values of E^* and f_1 for a conical tip ($\alpha = 2$).

$$f_1 = A_1 \mathfrak{s}(w) |H(w)|^{-1}, \tag{A6}$$

where

$$\mathfrak{s}(w) = \{(A_0/A_1)^2 - \sin^2[\angle H(w)]\}^{1/2} - \cos[\angle H(w)], \tag{A7}$$

and the transfer function of a fundamental flexural eigenmode of the cantilever is

$$H(w) = \frac{Q}{k} \frac{(1 - w^2/w_1^2)Q - iw/w_1}{(1-w^2/w_1^2)^2 Q^2 + w^2/w_1^2}, \tag{A8}$$

here k, Q, A_0, and w_1 are the cantilever stiffness, quality factor, free oscillation amplitude, and fundamental resonant frequency, respectively. Equations (A4) and (A6) tell us that for any given set of cantilever parameters and a set point amplitude, $F_{\max}$ and ξ are almost inversely proportional.

Equations (A2) and (A4) must be satisfied simultaneously. Therefore, we plot $F_{\max}/(\beta A_1^\alpha E)$ and $F_{\max}/f$ as a function of γ for differing values of E^* and f_1 in Fig. 4 to find a solution for a given sample elasticity. Here, E and $f = \beta A_1^\alpha E$ are the arbitrary values of E^* and f_1. An intersection of the curves gives the solution for γ and $F_{\max}$ values for a specific sample and a cantilever. No intersection means that there is no solution for the chosen cantilever. When $\gamma < -1$, it is found that $f_0 = F_{\max}(0.5+\gamma^2)/(1-\gamma)^2$, $f_1 = -2F_{\max}\gamma/(1-\gamma)^2$, $f_2 = 0.5F_{\max}/(1-\gamma)^2$ and $f_{n\geqslant 3} = 0$. Actually, f_1 is given by $-4\tan(\theta)E^* A_1^2 \gamma/\pi$ which increases for decreasing γ and hence there is always an intersection point.

Figure 5 is a sample plot of analytical and simulation results for the tip position and the interaction force. Although the two curves are very similar, they do not match each other perfectly. Since the enhanced second harmonic amplitude is about 17.5% of A_0 in this case, a small harmonic amplitude

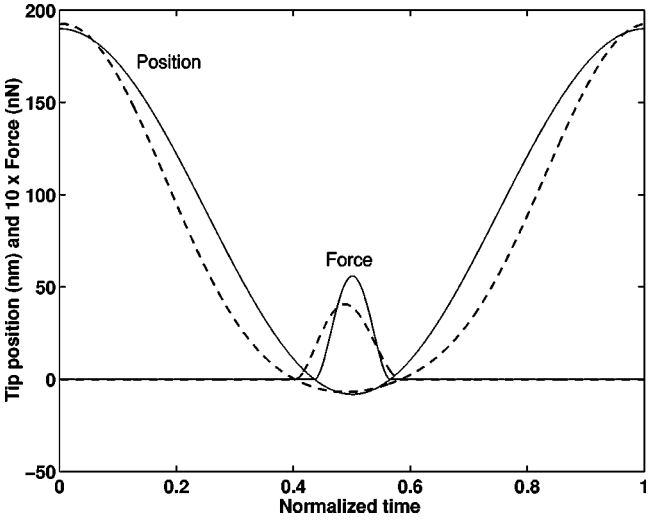

FIG. 5. Tip position and tip-sample interaction force in one cycle for a conical tip having a semivertical angle of $\theta=15°$ and a sample of $E^*=0.5$ GPa. The thin solid lines show the analytical solutions whereas the thick dashed lines indicate the simulation results. $A_0=100$ nm, $A_1/A_0=0.99$, $Q=100$, $k=1$ N/m, and $w=0.98w_1/2$. Notice that the interaction force is multiplied by 10 to fit into the figure.

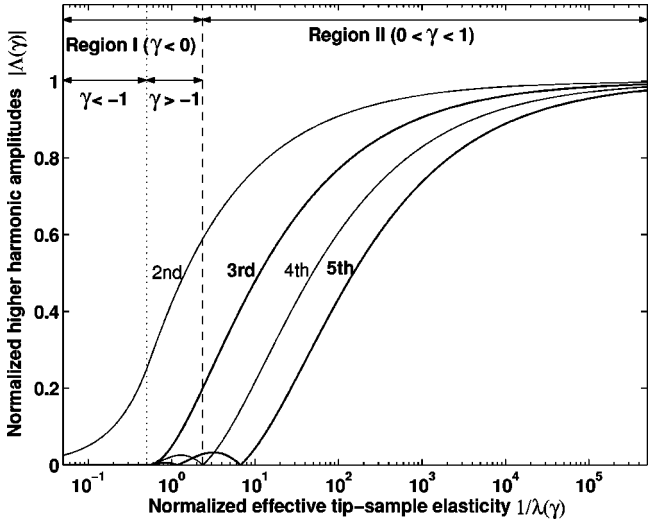

FIG. 6. A variation of the first four normalized harmonic amplitudes $|\Lambda(\gamma)|$ as a function of the normalized effective tip-sample elasticity $\lambda^{-1}(\gamma)$ for a conical tip ($\alpha=2$). It is assumed that $A_n \ll A_1$. Vertical dashed and dotted lines mark the $\gamma=0$ and $\gamma=-1$ locations.

approximation in an analytical derivation is violated and this deviation is to be expected. The two curves approach each other with smaller harmonic amplitudes.

Different sample elastic properties give rise to significantly different $F_{\max}$ and γ values. Although we are not able to measure any one of these parameters directly,[41] we can extract the sample elasticity by measuring the harmonic amplitudes. Notice that the constant term in Eq. (A1) depends on γ, but the feedback signal contains information on the height variations of the sample surface also.

We can relate the effective tip-sample elasticity to the nth harmonic amplitude by combining Eqs. (A2) and (A4) and utilizing $A_{n\geqslant 2}=|H(nw)f_n|$ as follows:

$$A_n=|(4/\pi)\tan(\theta)A_1^2H(nw)\xi h_n(\gamma)E^*|. \tag{A9}$$

There is no direct relation between A_n and E^* in Eq. (A9). However, ξ or γ can be used as an independent parameter to find respective A_n and E^* values. We can express A_n and E^* in terms of γ only,

$$A_n=|H(nw)A_1\varsigma(w)|H(w)|^{-1}\Lambda(\gamma)|, \tag{A10}$$

where $\Lambda(\gamma)$ is equal to $h_n(\gamma)/h_1(\gamma)$. Also $E^*=f_1/[\beta A_1^\alpha\lambda(\gamma)]$, where $\lambda(\gamma)$ is equal to $2\xi h_1(\gamma)$. Notice that as $\xi\to 0$, $\Lambda(\gamma)\to 1$ for which A_n reaches its maximum value $[\max(A_n)]$ and $\lambda(\gamma)\to 0$ for which E^* goes to infinity. In Fig. 6 we plot the first four normalized harmonic amplitudes $[A_n/\max(A_n)=|\Lambda(\gamma)|]$ as a function of the normalized effective tip-sample elasticity $[E^*\beta A_1^\alpha/f_1=\lambda^{-1}(\gamma)]$ under the assumption of a very small harmonic distortion ($A_n \ll A_1$). In this figure, the dashed vertical line marks the location of a $\gamma=0$ point.

The higher harmonic amplitudes show a monotonic increase in a wide range of sample compliance. Notice that the steeply increasing part of the amplitude curves shift towards a high Young's moduli region as the harmonic number increases. This makes one of the higher harmonics more preferable than the other ones depending on the sample. As the sample gets stiffer, A_n saturates since the variation of the contact time (and the penetration depth) gets smaller. This imposes an upper limit for measurable sample elasticity as reported earlier.[2] There is also a lower limit of E^* for which $\gamma>0$. Both limits can be shifted to the lower side of elasticity by softening the lever, by increasing the set point A_1/A_0 or oscillation amplitude, or by using a dull tip. The use of a dull tip is not preferable since it decreases the lateral image resolution. There is a practical maximum value of A_1/A_0 as determined by the precision of the feedback electronics. The oscillation amplitude can have an upper limit. Hence, the cantilever stiffness is the most suitable parameter to adjust the measurement region. The reverse procedure can be applied to shift the operation range to the high elasticity side. Note that changing these parameters also effect the maximum force applied to the surface $F_{\max}$. We recall that the attractive forces are assumed to be very small compared to $F_{\max}$ and increasing $F_{\max}$ too much can destroy the tip and/or the sample.

*Electronic address: mujdat@ee.bilkent.edu.tr

[1] N. A. Burnham and R. J. Colton, J. Vac. Sci. Technol. A **7**, 2906 (1989).
[2] P. Maivald, H. J. Butt, S. A. C. Gould, C. B. Prater, B. Drake, J. A. Gurley, V. B. Elings, and P. K. Hansma, Nanotechnology **2**, 103 (1991).
[3] U. Rabe, K. Janser, and W. Arnold, Rev. Sci. Instrum. **67**, 3281 (1996).
[4] K. Yamanaka and S. Nakano, Jpn. J. Appl. Phys., Part 1 **35**, 3787 (1996).
[5] N. A. Burnham, A. J. Kulik, G. Gremaud, P. J. Gallo, and F. Oulevey, J. Vac. Sci. Technol. B **14**, 794 (1996).
[6] W. Kiridena, V. Jain, P. K. Kuo, and G. Liu, Surf. Interface Anal. **25**, 383 (1997).
[7] D. DeVecchio and B. Bhushan, Rev. Sci. Instrum. **68**, 4498 (1997).
[8] R. W. Stark, T. Drobek, M. Weth, J. Fricke, and W. M. Heckl, Ultramicroscopy **75**, 161 (1998).
[9] A. Vinckier and G. Semenza, FEBS Lett. **430**, 12 (1998).
[10] K. Yamanaka and S. Nakano, Appl. Phys. A: Mater. Sci. Process. **66**, S313 (1998).
[11] A. Volodin, M. Ahlskog, E. Seynaeve, C. Van Haesendonck, A. Fonseca, and J. B. Nagy, Phys. Rev. Lett. **84**, 3342 (2000).
[12] E. Kester, U. Rabe, L. Presmanes, Ph. Tailhades, and W. Arnold, J. Phys. Chem. Solids **61**, 1275 (2000).
[13] S. Amelio, A. V. Goldade, U. Rabe, V. Scherer, B. Bhushan, and W. Arnold, Thin Solid Films **392**, 75 (2001).
[14] A. Touhami, B. Nysten, and Y. F. Dufrene, Langmuir **19**, 4539 (2003).
[15] T. R. Matzelle, G. Geuskens, and N. Kruse, Macromolecules **36**, 2926 (2003).
[16] S. Cuenot, C. Fretigny, S. D. Champagne, and B. Nysten, J. Appl. Phys. **93**, 5650 (2003).
[17] R. W. Stark and W. M. Heckl, Surf. Sci. **457**, 219 (2000).
[18] R. Hillenbrand, M. Stark, and R. Guckenberger, Appl. Phys. Lett. **76**, 3478 (2000).
[19] M. Stark, R. W. Stark, W. M. Heckl, and R. Guckenberger, Appl. Phys. Lett. **77**, 3293 (2000).
[20] O. Sahin and A. Atalar, Appl. Phys. Lett. **79**, 4455 (2001).
[21] S. J. T. van Noort, O. H. Willemsen, K. O. van der Werf, B. G. de Grooth, and J. Greve, Langmuir **15**, 7101 (1999).
[22] U. Dürig, New J. Phys. **2**, 5.1 (2000).
[23] T. R. Rodriguez and R. Garcia, Appl. Phys. Lett. **84**, 449 (2004).
[24] T. R. Rodriguez and R. Garcia, Appl. Phys. Lett. **80**, 1646 (2002).
[25] J. P. Cleveland, B. Anczykowski, A. E. Schmid, and V. B. Elings, Appl. Phys. Lett. **72**, 2613 (1998).
[26] R. W. Stark and W. M. Heckl, Rev. Sci. Instrum. **74**, 5111 (2003).
[27] O. Sahin, G. Yaralioglu, R. Grow, S. F. Zappe, A. Atalar, C. F. Quate, and O. Solgaard, Sens. Actuators, A **114**, 183 (2004).
[28] O. Sahin, C. F. Quate, O. Solgaard, and A. Atalar, Phys. Rev. B **69**, 165 416 (2004).
[29] O. Sahin and A. Atalar, Appl. Phys. Lett. **78**, 2973 (2001).
[30] M. Balantekin and A. Atalar, Appl. Surf. Sci. **205**, 86 (2003).
[31] L. Zitzler, S. Herminghaus, and F. Mugele, Phys. Rev. B **66**, 155 436 (2002).
[32] B. Anczykowski, B. Gotsmann, H. Fuchs, J. P. Cleveland, and V. B. Elings, Appl. Surf. Sci. **140**, 376 (1999).
[33] J. Tamayo and R. Garcia, Appl. Phys. Lett. **71**, 2394 (1997).
[34] R. Hegger, H. Kantz, and T. Schreiber, Chaos **9**, 413 (1999).
[35] M. Sano and Y. Sawada, Phys. Rev. Lett. **55**, 1082 (1985).
[36] J. P. Hunt and D. Sarid, Appl. Phys. Lett. **72**, 2969 (1998).
[37] R. W. Stark, Nanotechnology **15**, 347 (2004).
[38] J. P. Spatz, S. Sheiko, M. Möller, R. G. Winkler, P. Reineker, and O. Marti, Nanotechnology **6**, 40 (1995).
[39] H. Bielefeldt and F. J. Giessibl, Surf. Sci. **440**, L863 (1999).
[40] M. Balantekin and A. Atalar, Phys. Rev. B **67**, 193 404 (2003).
[41] M. Stark, R. W. Stark, W. M. Heckl, and R. Guckenberger, Proc. Natl. Acad. Sci. U.S.A. **99**, 8473 (2002).